The object of this study is Fe-Cr-Mn stainless steel alloys containing 0.23–0.41 wt.% C and 17.59–18.36 wt.% Cr with varying Mn content. The development of nickel-free stainless steels addresses the drawbacks of conventional implant materials such as titanium alloys, Co-Cr alloys, and AISI 316L stainless steel, which often suffer from biocompatibility issues, toxicity, and mechanical incompatibility with bone. The Fe-Cr-Mn alloys were produced by high-frequency induction melting and subsequently tested for microstructure, mechanical, wear, and corrosion properties. SEM-EDS revealed a transition from ferritic structure (2.5% Mn) to duplex α+γ (5% Mn) and predominantly austenitic structure (7.5% Mn). Mechanical testing showed that hardness and tensile strength peaked at 2.5% Mn, while ductility and impact toughness improved with increasing Mn, reaching their highest values at 5% Mn. Wear resistance increased significantly at higher Mn levels due to the formation of stable tribo-oxides and the strengthening effect of the austenitic matrix. Electrochemical testing in 0.9% NaCl solution showed that Fe-18Cr-5Mn possessed the best corrosion resistance, attributed to the stability of its passive film, while excessive Mn (7.5%) caused passivation breakdown through Mn-hydroxide formation. Overall, Fe-18Cr-5Mn exhibited the best synergy between strength, toughness, wear resistance, and corrosion protection under physiological saline conditions, establishing it as a promising nickel-free stainless steel for next-generation biomedical implant materials

Keywords: Fe-Cr-Mn alloys; implant materials; microstructure; mechanical properties; corrosion resistance; biocompatibility

UDC 669.14: 61
DOI: 10.15587/1729-4061.2025.341820

OPTIMIZATION OF Fe-Cr-Mn ALLOY COMPOSITION AS IMPLANT MATERIAL FOR MECHANICAL PROPERTIES AND CORROSION RESISTANCE

Ratna Kartikasari
Corresponding author
Doctor of Mechanical Engineering, Professor*
E-mail: ratna@itny.ac.id
Sugiarto Kadiman
Doktor of Electrical Engineering, Associate Professor**
Rivan Muhfidin
Master of Materials Science and Engineering, Assistance Professor*
Ihwanul Aziz
Master of Science, Researcher
Research Center for Accelerator Technology, Nuclear Energy Research Organization
National Research and Innovation Agency (BRIN)
Babarsari str., Caturtunggal, Sleman, Yogyakarta, Indonesia, 55281
*Department of Mechanical Engineering***
Department of Electrical Engineering*
***Institut Teknologi Nasional Yogyakarta
Babarsari str., Caturtunggal, Depok, Sleman, DIY, Indonesia, 55281

Received 31.07.2025
Received in revised form 03.10.2025
Accepted 13.10.2025
Published 30.10.2025

How to Cite: *Kartikasari, R., Kadiman, S., Muhfidin, R., Aziz, I. (2025). Optimization of Fe-Cr-Mn alloy composition as implant material for mechanical properties and corrosion resistance. Eastern-European Journal of Enterprise Technologies, 5 (12 (137)), 25–35. https://doi.org/10.15587/1729-4061.2025.341820*

1. Introduction

Implantable metallic materials are frequently utilized in medical devices, such as cardiovascular stents, dental prosthesis, and orthopedic implants, since they are strong, last a long time, and are cheap. Ti-based alloys, Co-Cr-Mo alloys, and stainless steel are the most commonly employed in clinical settings [1, 2]. These materials have many uses, but they also have some big problems that might cause bad biological reactions. For example, nickel can cause allergies, poisonous ions (Co/Cr) can be released, and Ti alloys don't match the elastic modulus of human bone [3, 4]. As a result, there has been a lot of interest in making stainless steels that don't include nickel and are cheap while yet having great mechanical, corrosion-resistant, and biocompatible properties [5].

The Fe-Cr-Mn alloy system is a good choice for implant materials because it has better mechanical properties, is more resistant to corrosion, and is less poisonous than other alloys. The creation of a CrO_3 oxide coating, which protects against corrosion better in hostile conditions like body fluids and physiological electrolytes, depends a lot on chromium (Cr) [6]. For biomedical uses that need high formability and resilience to fatigue, manganese (Mn) acts as an austenite stabilizer, making the material tougher and more ductile [7, 8]. The performance of Fe-Cr-Mn alloys as biomaterials can be enhanced by modifying the Mn content, thereby optimizing the balance of strength, corrosion resistance, and biocompatibility.

The mechanical characteristics of Fe-Cr-Mn alloys, such as tensile strength, hardness, and elongation, have been the subject of research. Mn stabilizes the FCC austenitic phase, which leads to higher ductility and better formability, particularly beneficial for implants that need to accommodate various loading conditions and long-term use. However, Cr improves the passivation layer, offering superior corrosion resistance in harsh and physiological conditions. It has been determined that a duplex structure ($\alpha + \gamma$) with the ideal Mn content, usually between 4 and 7%, provides the best strength and toughness combination [9, 10]. However, because less stable Mn-hydroxides are formed, higher Mn levels (> 7%) may decrease passivation stability and corrosion resistance [11].

As long as the Cr-rich passive film is preserved and the ion release (Cr and Mn) is regulated, the Fe-Cr-Mn alloys

have demonstrated low cytotoxicity and outstanding hemocompatibility in terms of biocompatibility. Despite being a necessary component of human metabolism, excessive Mn ion release from implants may cause neurotoxicity, as is the case with diseases like manganism. In order to prevent toxicity and preserve the necessary implant performance, it is imperative to optimize the Mn content to balance mechanical performance, corrosion resistance, and ion release [12].

Additionally, one of the most important factors influencing an alloy's suitability as an implant material is how it corrodes in physiological environments, such as saline solutions, Hank's solution, or Ringer's solution. The production of CrO_3 and $MnCrO_4$ films is essential for shielding the alloy from localized attacks and pitting corrosion. These films offer a thick, stable barrier that stops corrosion and ion release. But it's crucial to comprehend how changing the Mn content affects these alloys' electrochemical behavior and passivation stability, particularly when physiological ions are present [13].

In previous studies, Fe-Cr-Mn alloys were produced with Cr content ranging from 18%, C ranging from 1%, and Mn varying from 12–20% [14]. The results showed that the stiffness of these alloys was still too high compared to human bone, which remains a problem when these alloys are used as implants, as they interfere with the healing process [15]. The combination of mechanical properties, corrosion resistance, and biocompatibility of Fe-Cr-Mn alloys is highly dependent on the combination of Cr, Mn, and C compositions [13]. Therefore, studies devoted to understanding the influence of alloying elements, particularly manganese, on the microstructural evolution, mechanical response, corrosion resistance, and biocompatibility of Fe-Cr-Mn stainless steels are of high scientific relevance. Such investigations provide essential insights for developing advanced nickel-free stainless steels with mechanical compatibility to human bone and enhanced corrosion stability in physiological environments, thereby contributing to the progress of biomaterials engineering and the design of next-generation medical implants.

2. Literature review and problem statement

Metals used in medical implants, such as stainless steel (316L), Co-Cr-Mo, and Ti-6Al-4V, have been widely used due to their excellent mechanical strength and durability. However, these materials also have several disadvantages, such as allergic reactions to Ni in 316L, Co/Cr toxicity in Co-Cr alloys, and differences in elasticity with human bone in Ti alloys. Therefore, there is a need to find Ni-free implant metals that still have good biocompatibility, corrosion resistance, and mechanical strength but are more cost-effective [16].

One promising solution is the Fe-Cr-Mn alloy, which offers a good combination of biocompatibility, corrosion resistance, and mechanical strength. Chromium (Cr) in this alloy plays a role in forming a passive Cr_2O_3 layer that protects the alloy from corrosion, while manganese (Mn) acts as an austenite (FCC) phase stabilizer that provides toughness and ductility [17]. By varying the Mn content, the Fe-Cr-Mn alloy can be optimized to achieve a good balance between strength, corrosion resistance, and biocompatibility [18].

Fe-Cr-Mn alloys have several different crystal structures, including α (ferrite), γ (austenite), and σ (sigma phase), depending on the composition of Cr and Mn. Chromium plays an important role in the formation of a passive Cr_2O_3 layer, which provides protection against corrosion. On the other hand, manganese serves to stabilize the austenitic phase (FCC), which increases toughness and ductility, which are very important for implant applications that must withstand long-term loading and use. The optimal Mn content is usually between 4 to 7%, which produces a duplex structure ($\alpha + \gamma$), offering the best combination of strength and toughness [19]. However, higher Mn content (above 7%) can reduce passive stability and increase the likelihood of localized corrosion, which can affect material performance.

The mechanical properties of Fe-Cr-Mn alloys are greatly influenced by phase structure and grain size. The ferritic phase (α-BCC) tends to have higher strength but lower toughness compared to the austenitic phase (γ-FCC), which provides better toughness and formability. Chromium provides strengthening through solid solution strengthening, while manganese serves to stabilize the austenitic phase, which increases ductility and the ability to withstand deformation. Overall, the duplex structure ($\alpha + \gamma$) offers the best combination of strength, toughness, and corrosion resistance [18].

In addition, stacking fault energy (SFE) also affects the deformation mechanism in Fe-Cr-Mn alloys. Moderate SFE in these alloys allows for higher work hardening through twinning, which contributes to the ductility and strength of the alloy. Therefore, the Mn content is very important to achieve a good balance between strength, ductility, and work hardening [17, 19].

Corrosion is a major issue that needs to be considered in implant materials, especially in corrosive physiological environments. Chromium is the main element that forms the passive layer Cr_2O_3, which provides protection from corrosion in physiological media. Manganese helps to increase the stability of this passive layer by forming $MnCr_2O_4$ spinel and strengthening the passive film. At moderate Mn contents (around 4 to 7%), Fe-Cr-Mn alloys exhibit excellent corrosion resistance, especially against pitting corrosion and localized corrosion. However, at higher Mn contents, the passive layer can weaken, causing the alloy to be more susceptible to corrosion attack and ion release [20].

Research shows that annealing treatment of Fe-Cr-Mn alloys can help dissolve precipitates that can cause sensitization and improve the stability of the passive layer. Therefore, managing Mn content and proper surface treatment are very important for maintaining corrosion resistance in implant applications [21]. Although Fe-Cr-Mn has been extensively studied, many aspects still need further research, especially those related to the effect of Mn content on phase structure, mechanical properties, and corrosion resistance in physiological environments. The effect of Mn on passive film stability, as well as its relationship with ion release rate and biocompatibility, still requires further exploration. In addition, more in-depth research is needed on the optimization of Mn content to achieve the best balance between strength, toughness, corrosion, and biocompatibility.

Fe-18Cr-(12–20) Mn alloys belong to the duplex stainless-steel category, which has higher overall mechanical properties than SS316L. However, this also poses a problem because high rigidity can interfere with the healing process. In addition, the corrosion resistance and biocompatibility of Fe-Cr-Mn alloys still need to be improved to meet the material properties required for implants [14]. Efforts to find the right composition will lead to the discovery of targeted replacement alloys. Adjusting the composition of Cr, Mn, and C is the next step in obtaining the desired properties in

replacement alloys. Maintaining the Cr content to balance mechanical properties and corrosion resistance, adjusting the Mn content to promote austenite phase formation, and reducing the C content to a maximum of 0.25% to adjust mechanical properties are appropriate steps to provide alternative solutions for using Fe-Cr-Mn alloys as implant materials.

All this allows to assert that it is expedient to conduct a study on the effect of varying Mn content in Fe-18Cr-xMn alloys with controlled carbon levels to determine the optimal composition that provides the best combination of mechanical properties, corrosion resistance, and biocompatibility for biomedical implant applications. Such research is expected to fill the existing gap in understanding the correlation between Mn content, microstructural evolution, and electrochemical behavior, ultimately contributing to the development of cost-effective, nickel-free stainless steels for safe and reliable long-term use in the human body.

3. The aim and objectives of the study

The aim of this study is to identify the optimal manganese content within Fe-Cr-Mn alloys containing 0.23–0.41 wt.% C and 17.59–18.36 wt.% Cr that provides the best combination of mechanical properties and corrosion resistance for biomedical implant applications.

To achieve this aim, the following objectives were accomplished:

– to investigate the microstructure of the Fe-Cr-Mn alloys with varying Mn content;

– to examine the mechanical properties of the Fe-Cr-Mn alloys, including hardness, tensile strength, impact toughness and wear, as these properties determine how well the material can withstand the stresses placed on it in the body;

– to explore the corrosion resistance of these alloys, as corrosion behavior is a critical factor in the longevity of bone implants also evaluate how the variations in Mn content affect the passive film formation and corrosion rates of the alloys in physiological environments.

4. Materials and methods

The object of this study is Fe-Cr-Mn stainless steel alloys containing 0.23–0.41 wt.% C and 17.59–18.36 wt.% Cr with varying Mn content. Optimizing the Mn content in Fe-Cr-Mn alloys is expected to improve mechanical properties and corrosion resistance while ensuring that the material remains biologically compatible for long-term implant use. Mn is known for its austenite stabilization properties and ability to enhance the toughness and ductility of alloys. Meanwhile, Cr plays a key role in forming a protective Cr_2O_3 passive film, which is crucial for corrosion resistance in physiological environments.

The main hypothesis of this study is Fe-Cr-Mn alloy can be effectively used as non-toxic bone implants, without negatively affecting the healing process. Additionally, the hypothesis posits that these alloys, despite their increased Mn content, will exhibit mechanical properties sufficient to withstand the stresses typically encountered in bone replacement, without compromising the natural healing process.

Several assumptions have been made in the course of this study to ensure the consistency and reliability of the results. These include:

– the melting process is assumed to be perfect, with complete alloy homogeneity and no formation of casting defects;

– the materials used in the study are assumed to be uniformly mixed and free from impurities that might affect the final properties of the alloy.

The study simplification included the following: for the corrosion tests, a simplified solution of 0.9% NaCl is used to simulate the physiological environment and evaluate the corrosion resistance of the alloy.

The research was conducted using an 80 kg high-frequency induction chamber for melting the Fe-Cr-Mn alloys. The raw materials used in the alloy preparation included Fe-Cr LC, Fe-Mn MC, Fe-Si, and SUS 430 scrap. The Fe-Cr-Mn alloy castings were formed as ingots with dimensions of $30 \times 30 \times 200$ mm. To assess the chemical composition of the alloy, an inductively coupled plasma optical emission spectrometer (ICP-OES) was employed. The chemical compositions of the tested specimens are presented in Table 1. The annealing process was carried out at 900°C for 1 hour in a muffle furnace to homogenize the alloy structure.

Several tests were conducted to evaluate the properties of the Fe-Cr-Mn alloys, including chemical composition, microstructure, hardness, tensile strength, impact toughness, wear and corrosion resistance. The chemical composition of each alloy was analyzed using a Baird FSQ foundry spectrovac spectrometer, following ASTM E2209 standards. This spectrometric method ensures accurate determination of elemental composition in metallic samples, verifying that the desired Mn levels (2.5, 5, and 7.5 wt.%) were achieved. The microstructure of the alloys was examined using a JEOL JSM-6360LA Scanning Electron Microscope (SEM) equipped with an Energy Dispersive X-ray Spectroscopy (EDS) system. SEM-EDS analysis was performed to observe grain morphology, phase distribution, and elemental composition of the matrix. The observations provided information about the phase transformation from ferritic to austenitic structures with increasing Mn content. Hardness testing was conducted using a Schmierplan/Libriction LA-H-250 RC 16-02 tester employing the macro-Vickers method, in accordance with ASTM E92 standards. A diamond indenter with a fixed load was used to determine the macrohardness of each alloy, which reflects the alloy's resistance to localized plastic deformation. Tensile testing was conducted using a TN 20 MD Controlab tensile testing machine based on ASTM E8 standards. The test specimens were prepared with standard gauge dimensions, and the resulting stress-strain data were used to determine ultimate tensile strength and elongation. Impact testing was performed using the Charpy method, in compliance with ASTM E23 07 A standards. The tests were conducted on notched specimens to measure the absorbed energy during fracture, providing insight into the material's ability to resist sudden impact loading. Wear resistance was evaluated using the Ogoshi-type wear testing machine based on ASTM G99-95A standards. The test was conducted under dry sliding conditions with a fixed load and speed to determine wear rate. The wear tracks were examined after testing to identify the wear mechanisms and the role of Mn in forming protective tribo-oxide layers. Corrosion resistance was evaluated using the CMS 100 Gamry Instrument corrosion polarization test in a 0.9% NaCl solution, with polarization potential measurements determined according to ASTM G5 standards. The corrosion potential (*Ecorr*), current density (*Icorr*), and passive film stability were analyzed to evaluate the corrosion resistance of each alloy composition.

Table 1

The chemical composition of Fe-Cr-Mn alloy

Elements / %wt	Fe	Cr	Mn	C	Si	S	P
2.5	Bal.	18.36	2.89	0.23	0.57	0.008	0.05
5	Bal.	17.8	5.2	0.41	1.09	0.008	0.05
7.5	Bal.	17.59	8.07	0.41	1.18	0.002	0.05

The Fe-Cr-Mn's chemical makeup is shown in Table 1. The levels of Cr, C, and Mn were changed during the alloy-making process in order to fulfill the research objective of determining how increasing the Mn levels impacts the various features under investigation. The Fe content decreased while the Mn content increased.

5. Results of Fe-Cr-Mn alloy characteristics

5. 1. Results of the microstructure of Fe-Cr-Mn alloys

5. 1. 1. Results of the scanning electron microscope of Fe-Cr-Mn alloys

Fig. 1 shows the results of microstructure testing of Fe-Cr-Mn alloys.

The microstructures in Fig. 1, *a*, *b* show a background (homogeneous dark field) indicating a dominant ferritic matrix phase (α-Fe). Needle-like/lath precipitates are visible scattered throughout the matrix. In Fig. 1, *c*, *d*, the surface appears relatively homogeneous compared to the previous Fe-Cr-2.5Mn alloy. The fine crystal grain pattern indicates the dominance of the ferrite phase (α-Fe), but with a higher Mn content (5%), the Mn-stabilized austenite phase (γ-Fe) may begin to appear. Clearer grain boundaries are visible. In the Fe-Cr-5Mn alloy, large rod-shaped precipitates like those in Fe-Cr-2.5Mn are not visible [17, 18].

The surface of the Fe-Cr-7.5Mn alloy (Fig. 1, *e*, *f*) shows a relatively smooth surface but with slip bands within the grains. In the Fe-Cr-7.5Mn alloy, the matrix likely consists of a dominant mixture of austenite with some ferrite (a duplex structure tending toward austenitic). There is an accumulation of coarse precipitates around the grain boundaries, forming precipitate agglomerations. The grain boundaries are clearly visible with concentrated precipitation along the boundary lines [6].

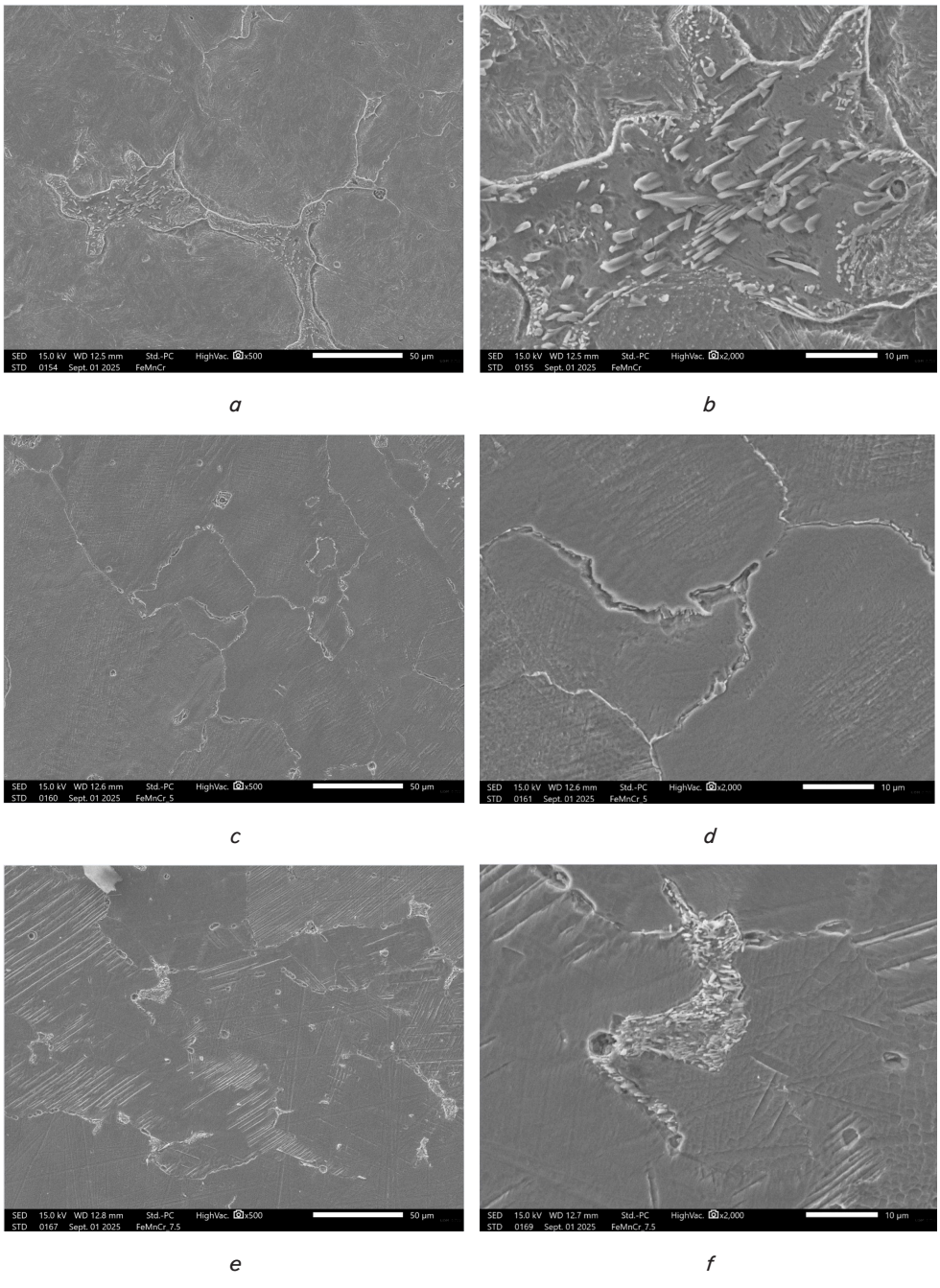

Fig. 1. Microstructure of Fe-Cr-Mn alloys: *a, b* – 2.5 Mn; *c, d* – 5 Mn; *e, f* – 7.5 Mn

5. 1. 2. Results of the energy dispersive spectroscopy of Fe-Cr-Mn alloys

Fig. 2 shows the results of energy dispersive spectroscopy testing of Fe-Cr-Mn alloys.

The Fe-Cr-2.5Mn alloy (Fig. 2, *a*) shows a composition dominated by Fe, with the main alloying elements being Cr at around 10 at.% and Mn at around 7 to 8 at.%. The Mn content is still relatively low, so that the distribution of elements in the matrix appears more homogeneous without significant segregation. The presence of Mn at this level plays a role in strengthening the solid solution but is not high enough to form Mn-rich phase precipitation. Minor peaks of O and Si elements indicate the possibility of surface contamination or thin oxide phase residues due to the sample preparation process [18]. Fig. 2, *b* shows that the Mn content increases to around 14 to 15 at.%, while Fe decreases and Cr decrease slightly in the range of 8 to 9 at.%. Mn distribution is more pronounced in the alloy, which may indicate the formation of Mn-rich regions or small precipitates at the grain boundaries. The Fe-Cr-7.5Mn alloy (Fig. 2, *c*) shows a further increase in Mn content to around 17 to 18 at.%, with Fe decreasing and Cr remaining in the range of 8 to 9 at.%. High Mn content has the potential to trigger more pronounced segregation and the formation of Mn-rich phases [8, 22].

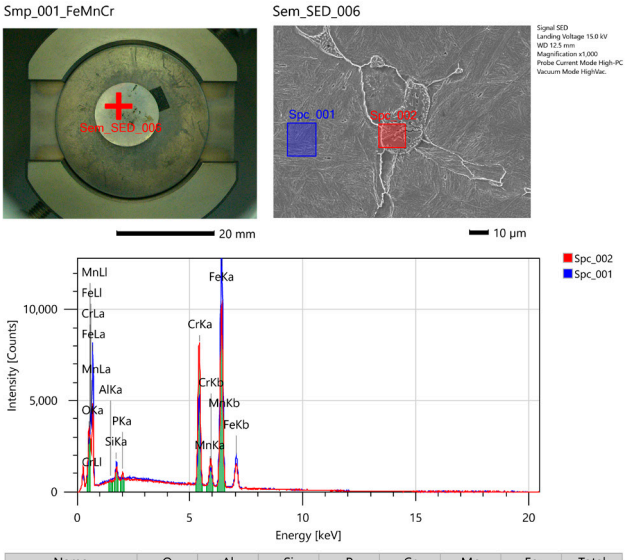

Name	O	Al	Si	P	Cr	Mn	Fe	Total
Spc_002	1.86	0.09	0.63	0.50	28.64	3.05	65.24	100.00
Spc_001			0.75		16.18	2.35	80.73	100.00
Average	1.86	0.09	0.69	0.50	22.41	2.70	72.98	
Standard Deviation			0.06		6.23	0.35	7.75	

Atom/Mol%

a

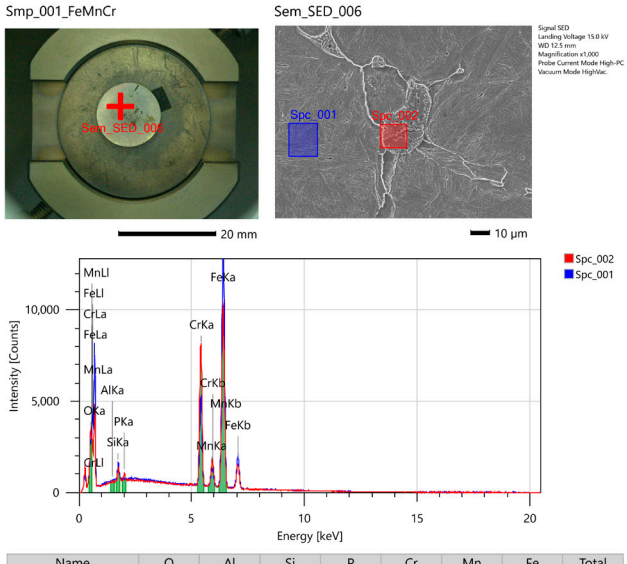

Name	O	Al	Si	P	Cr	Mn	Fe	Total
Spc_002	1.86	0.09	0.63	0.50	28.64	3.05	65.24	100.00
Spc_001			0.75		16.18	2.35	80.73	100.00
Average	1.86	0.09	0.69	0.50	22.41	2.70	72.98	
Standard Deviation			0.06		6.23	0.35	7.75	

Atom/Mol%

b

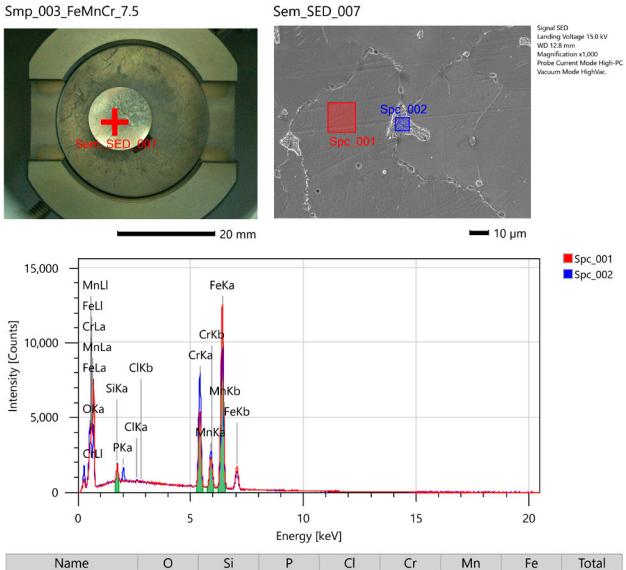

Name	O	Si	P	Cl	Cr	Mn	Fe	Total
Spc_001		0.93			16.93	7.58	74.56	100.00
Spc_002	2.28	0.99	1.07	0.17	27.14	9.19	59.15	100.00
Average	2.28	0.96	1.07	0.17	22.04	8.38	66.86	
Standard Deviation		0.03			5.10	0.81	7.70	

Atom/Mol%

c

Fig. 2. The SEM-EDS micrograph of Fe-Cr-Mn where: *a* – 2.5 Mn; *b* – 5 Mn; *c* – 7.5 Mn

5. 2. Results of the mechanical properties of Fe-Cr-Mn alloys

5. 2. 1. Results of the hardness of Fe-Cr-Mn alloys

The hardness distribution of Fe-Cr-Mn alloy with various weight % of Mn presented in Fig. 3.

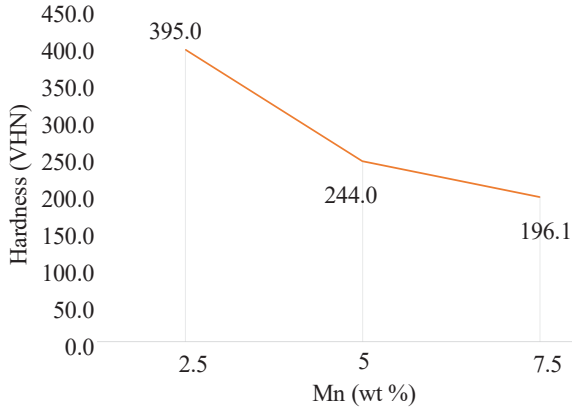

Fig. 3. The hardness distribution of Fe-Cr-Mn alloy

The hardness value of 395.0 VHN at a Mn content of 2.5% drops by 38.2% at a Mn content of 5% to 244.0 VHN, and it further drops by 19.6% at a Mn content of 7.5% to 196. Fig. 3 illustrates how the hardness of Fe-Cr-Mn alloys drops dramatically with increasing Mn content. This downward trend is in line with the phase evolution that the Fe-Cr-Mn ternary diagram predicted for Cr in the range of 18%, specifically the transition from phase α (ferrite) to $\alpha+\gamma$ (duplex) at 5% Mn and to γ (austenite) at 7.5% Mn. At 2.5% Mn, the microstructure is dominated by the ferrite phase (BCC) with the possibility of Cr-rich particles at the grain boundaries (M23C6), resulting in strengthening through solid solution and precipitation with relatively small grain sizes, all of which increase hardness [23]. At 5% Mn, a duplex $\alpha+\gamma$ structure forms, and the presence of a softer austenite fraction lowers the average hardness value, although the total tensile strength may remain good due to the hardness of γ. At 7.5% Mn, austenite (FCC) dominates and tends to coarsen during soaking, causing hardness to decrease further. This decrease in hardness is also in line with the Hall-Petch theory, where grain enlargement reduces strength/hardness [2]. EDS data shows higher Mn in the matrix (γ characteristic) and higher Cr at the grain/particle boundaries (α/Cr-rich carbide characteristic). At 2.5% Mn, strong Cr enrichment is observed at the grain boundaries (strengthening), while at 7.5% Mn, the Mn-rich (γ) matrix is softer, both of which explain the measured decrease in hardness [24].

5. 2. 2. Results of the tensile strength of Fe-Cr-Mn alloys

The result of tensile test of Fe-Cr-Mn alloy with various weight % of Mn presented in Fig. 4, 5. Fe-Cr-Mn alloy castings' tensile strength dropped precipitously by 43.5%, from 724.41 MPa at 2.5% Mn to 409.54 MPa at 5% Mn, before dipping marginally by 6.2% to 384.27 MPa at 7.5% Mn. Tensile strength dropped by 47% over time. Additionally, the elongation dropped from 8.88% at 2.5% Mn to 6.35% at 5% Mn and 6.18% at 7.5% Mn. The largest decrease, 28.5%, occurred between 2.5% and 5% Mn, accounting for 30.4% of the total decrease. This pattern is consistent with hardness values decreasing as Mn content rises [25]. The highest tensile strength and strain occur at a Mn content of 2.5%, where the α-ferrite matrix has relatively fine grain size and Cr-Mn solid solution strengthening, plus the possibility of moderate amounts of Cr-rich particles (M23C6). At 5% Mn, tensile strength and strain decrease sharply due to the formation of the $\alpha+\gamma$ duplex phase. The introduction of a softer γ fraction reduces the average tensile strength, while Cr-rich precipitates/grain boundaries visible in SEM–EDS limit strain (Cr→α/GB partition, Mn→γ/matrix) [25]. These results are consistent with reports that Mn stabilizes γ, but at medium levels and low C/N, work-hardening is not sufficient to prevent strength reduction [26]. At 7.5% Mn, a further but more gradual decrease occurs where the γ-austenite phase dominates; the coarsening tendency during soaking reduces tensile strength (weakening of Hall-Petch). Strain recovery is not significant because Ni-free austenite with 7.5% Mn and low C/N does not achieve the TRIP/TWIP mechanism, which typically requires much higher Mn and controlled stacking fault energy (SFE).

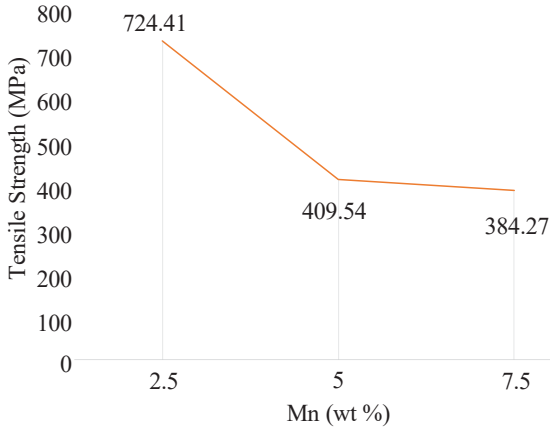

Fig. 4. The tensile strength of Fe-Cr-Mn alloy

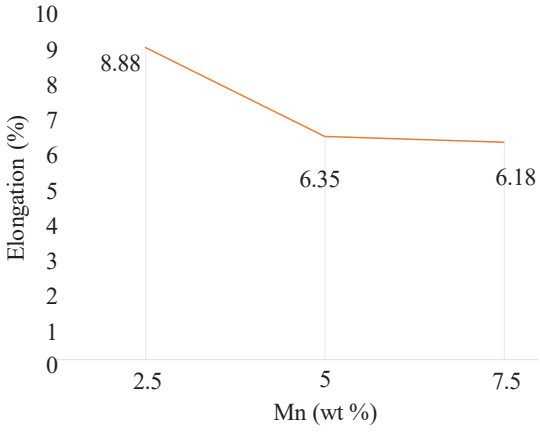

Fig. 5. The elongation of Fe-Cr-Mn alloy

Fig. 6 shows that the fracture surface of the Fe-Cr-2.5Mn alloy appears rough with many small, irregular dimples. This indicates a ductile fracture mechanism, although the distribution of dimples shows uneven plastic deformation.

The fracture surface shows deeper and more uniform dimples, with a clearer fracture pattern resembling microvoid coalescence. This indicates an increase in plastic deformation prior to fracture, which is consistent with a decrease in hardness (244 VHN) and an increase in austenite phase stabilization due to higher Mn content. The fracture surface tends to be smoother with elongated dimples and the presence of shear lips, which are characteristics of dominant ductile fracture. The high Mn content stabilizes the γ austenite, thereby increasing deformability, although it results in a decrease in hardness (196 VHN) [4, 27].

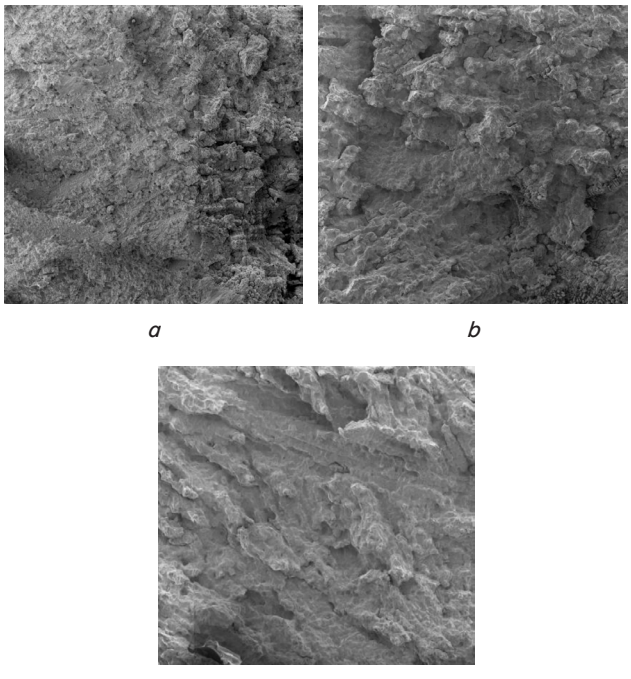

a *b* *c*

Fig. 6. The Macro photograph of the fracture surface resulting from tensile testing of Fe-Cr-Mn alloy: *a* – 2.5 Mn; *b* – 5 Mn; *c* – 7.5 Mn

5. 2. 3. Results of the impact of Fe-Cr-Mn alloys

The result of impact test of Fe-Cr-Mn alloys with various weight % of Mn presented in Fig. 7.

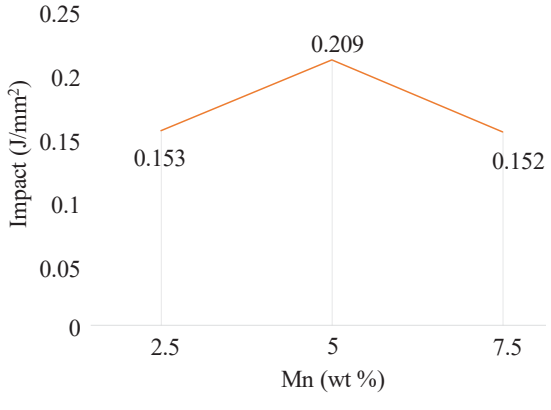

Fig. 7. The impact of Fe-Cr-Mn alloy

The impact energy of the Fe-Cr-Mn alloy increased by 36.6% from 0.153 J/mm^2 at 2.5% Mn to 0.209 J/mm^2 at 5% Mn, then decreased by 27.3% to 0.152 J/mm^2 at 7.5% Mn. The highest value occurred at 5% Mn. The Fe-Cr-Mn alloy with 2.5% Mn is in the α-ferrite (BCC) region. SEM-EDS test results show Cr enrichment at grain boundaries (indicating M23C6/early occurrence of σ phase). Cr-rich particles at grain boundaries are embrittling, resulting in low impact energy [24]. Fe-Cr-Mn alloys with 5% Mn content are in the duplex zone ($\alpha + \gamma$). The presence of austenite phase (γ, FCC) distributed between grains bridges cracks, deflects crack paths, and increases toughness, resulting in maximum impact energy. The Mn boundary pattern in γ and Cr in α from EDS confirms this. Fe-Cr-Mn alloys with 7.5% Mn are dominated by γ-austenite. Although γ is generally ductile, in low-Ni systems with medium-high SFE and coarse grains, twinning/TRIP is inactive and work-hardening is low; if carbides/σ are still present at the grain boundaries, toughness falls back, so that impact energy approaches the value for 2.5% Mn [28].

The fracture surface of the Fe-Cr-Mn alloy impact test specimen in Fig. 8.

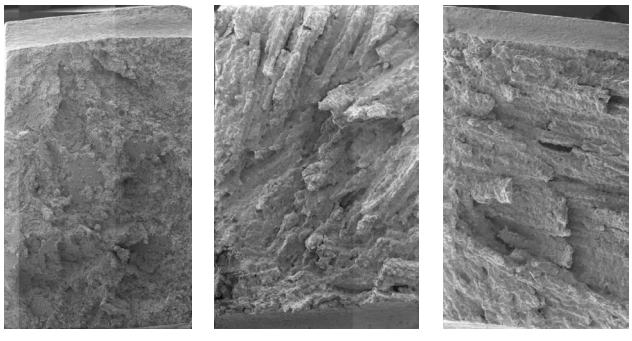

a *b* *c*

Fig. 8. Macro photograph of the fracture surface of the Fe-Cr-Mn alloy after impact testing: *a* – 2.5 Mn; *b* – 5 Mn; *c* – 7.5 Mn

Fig. 8, *a* shows that the fracture surface of the Fe-Cr-2.5Mn alloy (*a*) is relatively flat with a granular area, indicating the dominance of brittle fracture. Impact absorption energy in this condition is likely to be low due to limited plastic deformation. The Fe-Cr-5Mn alloy (Fig. 8, *b*) has a fracture surface combining brittle and ductile areas, with a pattern of elongated grooves and shear planes [27]. This indicates a transition from brittle behavior to mixed fracture. Higher Mn content stabilizes the austenite phase, increasing ductility and plastic deformation when subjected to shock loading. The Fe-Cr-7.5Mn alloy (Fig. 8, *c*) shows a fracture surface dominated by elongated grooves and a fibrous fracture pattern, characteristic of ductile fracture. The presence of a fibrous pattern indicates significant plastic deformation before fracture, signifying an increase in the material's ability to absorb impact energy. This is consistent with the role of high Mn in increasing toughness through the stabilization of γ austenite [28].

5. 2. 4. Results of the wear of Fe-Cr-Mn alloys

The result of wear test of Fe-Cr-Mn alloys with various weight % of Mn presented in Fig. 9.

The wear value of the Fe-Cr-Mn alloy (Fig. 9) decreased sharply by 46.7% when Mn was increased from 0.000454 (2.5% Mn) to 0.000242 (5% Mn) and decreased again by 60.3% to 0.000096 when Mn was increased to 7.5%. The total wear reduction was 78.8% when Mn was increased from 2.5% to 7.5%, meaning that wear resistance increased significantly with increasing Mn. This is due to phase evolution where, at 18% Cr, an increase in Mn shifts the microstructure from α (BCC) to $\alpha + \gamma$ (duplex) and then to γ (FCC). The continuous γ matrix at 7.5% Mn provides better resistance to friction and reduces delamination/microcracks during sliding, thereby reducing the wear rate [29]. According to Archard, wear volume $= \propto (k \cdot W \cdot L) / H$. At 2.5% Mn, H is high but k is large because Cr-rich (σ) precipitates at the grain boundaries cause delamination and microploughing. At 5 to 7.5% Mn, the separation of Mn (γ) and Cr (α) makes the grain boundaries more perfect and k decreases; the result is less wear despite lower hardness. Mn-rich austenite tends to undergo work hardening under the influence of friction and form stable tribo-oxides (e. g., Mn-Cr spinel) that act as

a protective layer/MML (mechanically mixed layer), reducing friction and wear [30]. A more homogeneous duplex/austenitic microstructure distributes loads and deflects crack paths, resulting in finer and more stable debris that reduces third-body abrasion.

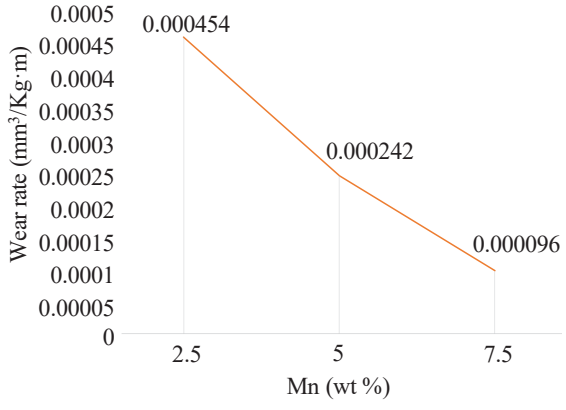

Fig. 9. The wear of Fe-Cr-Mn alloy

5. 3. Results of the corrosion resistance of Fe-Cr-Mn alloys

The result of corrosion test of Fe-Cr-Mn alloys with various weight % of Mn presented in Fig. 11. The polarization curve can be seen in Fig. 10.

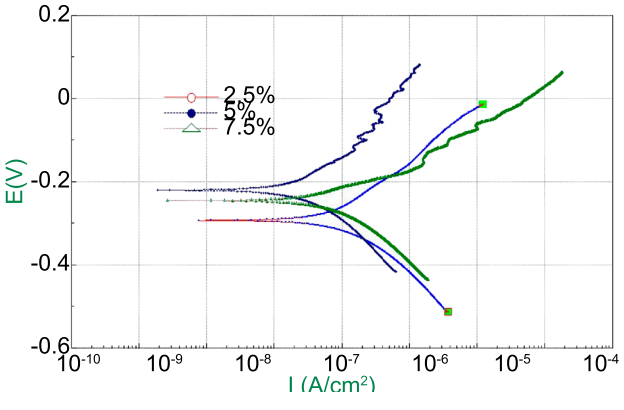

Fig. 10. The polarization curve of Fe-Cr-Mn alloy

Fig. 11 shows that the corrosion rate of the Fe-Cr-Mn alloy decreased sharply from 0.003198 mm/year at 2.5% Mn to 0.001230 mm/year at 5% Mn (a significant decrease of 61.6%), then increases again to 0.001923 mm/year at 7.5% Mn (an increase of 56.3% compared to 5% Mn, still around 40% lower than 2.5% Mn). The polarization curve (Fig. 10) shows that at 5% Mn, the curve shifts to a more noble potential (E-corr is more positive) and the corrosion current (i-corr) is smaller, with a wider passive range indicating a dense and stable passive film. At 7.5% Mn, i-corr increases again, causing the corrosion rate to rise. SEM-EDS test results show that alloys with a Mn content of 2.5% have a structure dominated by ferrite (α) and show indications of Cr enrichment at the grain boundaries. Fe-Cr-Mn alloys with 18% Cr readily form $M_{23}C_6$ carbides (σ-phase) at 600–900°C. Local Cr depletion around grain boundaries weakens the formation of Cr_2O_3, resulting in less stable passivation and high i_corr [12]. Fe-Cr-Mn alloys with 5% Mn have a duplex ($\alpha+\gamma$) structure where element partitioning (Mn→γ, Cr→α) creates a more balanced matrix and grain boundaries, reducing the Cr depletion zone. Furthermore, Mn contributes to the $MnCr_2O_4$/MnO spinel within/above Cr_2O_3, which compacts and stabilizes the passive film, thereby reducing i-corr [31]. At 7.5% Mn, the structure is dominated by the γ-austenite phase. Excess Mn can dilute effective Cr in the matrix/film and produce more soluble Mn hydroxide, resulting in a less stable passive film and increased i-corr; on the other hand, γ grains that tend to coarsen accelerate local initiation. As a result, corrosion resistance decreases relative to 5% Mn, but remains better than 2.5% Mn.

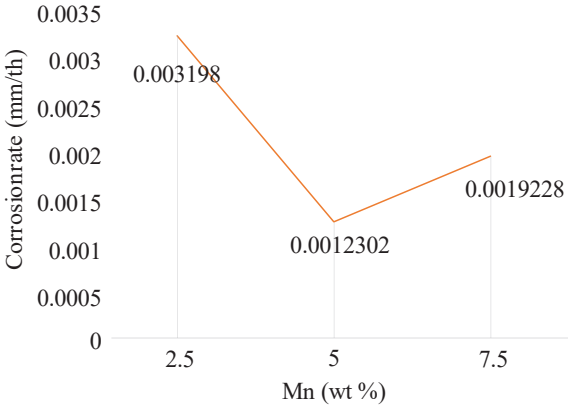

Fig. 11. The corrosion rate of Fe-Cr-Mn alloy

6. Discussion of results of Fe-Cr-C with high Mn characteristics

The SEM-EDS analysis (Fig. 1) revealed that the microstructure of Fe-Cr-Mn alloys strongly depends on Mn content. At 2.5% Mn, the alloy was dominated by α-ferrite with Cr-rich precipitates along grain boundaries, identified as $M_{23}C_6$ carbides. Such precipitates are known to cause localized Cr depletion, thereby embrittling grain boundaries, consistent with previous observations in Ni-free stainless steels [17]. At 5% Mn (Fig. 1, *b*), a duplex structure ($\alpha+\gamma$) formed, with Mn partitioning into γ and Cr into α. This balanced distribution improved microstructural stability and reduced carbide precipitation, consistent with observations by [31]. At 7.5% Mn, γ-austenite became dominant (Fig. 1, *c*), but coarse grains and residual precipitates reduced microstructural stability, confirming similar findings in high-Mn steels [8].

These structural alterations were followed by mechanical properties. Due to carbide hardening and ferritic strengthening [32], hardness (Fig. 2) and tensile strength (Fig. 3) were high at 2.5% Mn, while toughness (Fig. 7) was low. At 5% Mn, where γ-austenite helped with fracture deflection and energy absorption, the greatest impact toughness was attained. This is in line with the findings of Nayak et al. [8], who found that balanced duplex structures improve toughness without compromising resistance to corrosion. Although γ-austenite is typically ductile at 7.5% Mn, its coarse grain size and lack of TRIP/TWIP processes resulted in lower strength and less work-hardening, which is consistent with Hall-Petch softening behavior [26].

Fractography supported these observations (Fig. 6, 8). The alloy with 2.5% Mn showed shallow dimples and quasi-cleavage features, indicating brittle fracture. The 5% Mn alloy exhibited deeper and more uniform dimples, confirming higher ductility through microvoid coalescence. At 7.5% Mn, elongated dimples suggested ductile fracture but with diminished resistance to crack propagation. These results mirror [12], who reported that austenite-dominated steels require active defor-

mation mechanisms to sustain toughness, which are absent in medium-Mn, Ni-free systems.

Additionally, there was a non-linear correlation between corrosion resistance and Mn concentration (Fig. 11). Because of Cr-depleted zones brought on by carbide precipitation, which destabilized the passive film, the alloy containing 2.5% Mn demonstrated poor corrosion performance. According to [12], a stable passive layer comprising Cr_2O_3 and $MnCr_2O_4$ spinels is responsible for the 5% Mn alloy's superior corrosion resistance. Passivation stability was decreased by additional Mn addition to 7.5%, most likely as a result of the production of soluble Mn oxides and a relative decrease in Cr in the passive film. [27] shown that too much Mn decreases passive film protectiveness in chloride-rich conditions, which is in line with this observation.

Microstructure and hardness affected wear behavior. While the 5% Mn alloy showed a compromise between wear resistance and ductility, the 2.5% Mn alloy, which had a higher hardness, showed superior wear resistance. Reduced hardness and a preponderance of soft γ-austenite caused the wear resistance to diminish at 7.5% Mn. Similar trade-offs between wear resistance and hardness have been documented in other Ni-free stainless steels [17], indicating that tribological and mechanical parameters must be balanced within an ideal Mn range.

The best combination of characteristics is found in Fe-Cr-Mn alloys at 5% Mn, where a duplex $\alpha+\gamma$ structure improves toughness and corrosion resistance while preserving respectable strength and wear resistance. While alloys with 7.5% Mn exhibit enhanced ductility but diminished strength and corrosion stability, those with 2.5% Mn exhibit increased hardness but poor toughness and corrosion behavior. Based on these results, which are consistent with previous advances in Ni-free stainless steel [2, 4], the controlled addition of approximately 5% Mn can be recommended for further development to meet the needs of biomedical applications where biocompatibility and mechanical reliability are critical.

The results obtained in this study have direct practical relevance for the design and development of nickel-free stainless steels for biomedical implant applications. The Fe-Cr-5Mn alloy, which exhibited the most balanced combination of strength, ductility, wear resistance, and corrosion protection, can be applied in the production of orthopedic and dental implants, particularly where biocompatibility and corrosion resistance in physiological environments are essential. The optimal composition minimizes the risk of allergic reactions and ion toxicity associated with nickel-containing steels, while maintaining sufficient mechanical integrity for long-term load-bearing use. Under typical physiological conditions, such as exposure to saline body fluids (0.9% NaCl), the alloy demonstrates stable passivation behavior, indicating good performance in in vivo environments. The potential effects of applying this material include enhanced implant longevity, reduced post-surgical complications, and improved patient safety. Furthermore, the findings may guide future industrial alloy design and heat-treatment optimization for biomedical-grade stainless steels.

Despite the promising results, this study has several limitations. The alloys were investigated in the as-cast condition, which may affect microstructural homogeneity and consequently influence the mechanical and corrosion responses; future work should therefore include homogenization through annealing to minimize segregation. Moreover, while corrosion resistance trends were observed, a more detailed electrochemical analysis under various physiological media is still required to validate passivation stability. Importantly, biocompatibility tests have not yet been conducted, which are essential to confirm the suitability of these alloys for biomedical applications. Thus, future studies should focus on post-casting heat treatment, advanced electrochemical characterization, and comprehensive in vitro/in vivo biocompatibility evaluations to establish the full potential of Fe-Cr-Mn alloys as Ni-free implant materials.

7. Conclusions

1. The microstructure of Fe-Cr-Mn alloys is significantly influenced by Mn: 2.5% Mn favors α-ferrite with carbide precipitation, 5% stabilizes a duplex $\alpha + \gamma$ structure, and 7.5% promotes γ-austenite with grain boundary segregation.

2. The highest toughness (0.209 J/mm^2) and balanced ductility occur at 5% Mn, while the highest hardness (395 VHN) and tensile strength (724 MPa) occur at 2.5% Mn. Strength declines and ductile fracture take over at 7.5% Mn. The addition of Mn greatly increases wear resistance; the best performance occurs at 7.5% Mn because of the stable tribo-oxide formation and work hardening of the γ-matrix.

3. Stable CrO_3-$MnCrO_4$ passive films support corrosion resistance, which peaks at 5% Mn. Because of Mn-hydroxide segregation and carbide formation, respectively, lower (2.5%) and higher (7.5%) Mn contents decrease passivation stability.

The best option for Ni-free stainless-steel implant materials is Fe-Cr-Mn with 5% Mn since it offers the best overall balance of strength, toughness, wear resistance, and corrosion protection.

Conflict of interest

The authors declare that they have no conflict of interest in relation to this study, whether financial, personal, authorship or otherwise, that could affect the study and its results presented in this paper.

Financing

The study was funded by the Ministry of Higher Education, Science, and Technology, Republic of Indonesia by "Regular Fundamental Research Grants" under Decree number: 0419/C3/DT.05.00/2025 May 22th 2025, 126/C3/DT.05.00/PL/2025 May 28th 2025, 0498.30/LL5-INT/AL.04/2025 Jun 4th 2025 and 02/ITNY/LPPMI/Pen.DPPM/PFR/VI/2025 Jun 12th 2025.

Data availability

Data will be made available on reasonable request.

Use of artificial intelligence

The authors confirm that they did not use artificial intelligence technologies when creating the current work.

Acknowledgments

The authors would like to thank the Ministry of Higher Education, Science, and Technology, Indonesia, which has funded this research through the Regular Fundamental Grant program in 2025.

References

1. Borgioli, F., Galvanetto, E., Bacci, T. (2021). Surface Modification of a Nickel-Free Austenitic Stainless Steel by Low-Temperature Nitriding. Metals, 11 (11), 1845. https://doi.org/10.3390/met11111845
2. Pani, R., Behera, R. R., Roy, S. (2023). Corrosion Behaviour of Metallic Biomaterials in Physiological Environments. Handbook of Research on Corrosion Sciences and Engineering, 246–273. https://doi.org/10.4018/978-1-6684-7689-5.ch009
3. Radice, S., Neto, M. Q., Fischer, A., Wimmer, M. A. (2021). Nickel-free high-nitrogen austenitic steel outperforms CoCrMo alloy regarding tribocorrosion in simulated inflammatory synovial fluids. Journal of Orthopaedic Research, 40 (6), 1397–1408. https://doi.org/10.1002/jor.25174
4. Ansary, S., Mondal, S., Sekh, M., Haque, R., Haidar, S. (2022). Indigenous Production of Porous 316L through Powder Metallurgy and Investigation of their Mechanical Properties. Key Engineering Materials, 933, 32–41. https://doi.org/10.4028/p-2fqtl1
5. Patnaik, L., Ranjan Maity, S., Kumar, S. (2020). Status of nickel free stainless steel in biomedical field: A review of last 10 years and what else can be done. Materials Today: Proceedings, 26, 638–643. https://doi.org/10.1016/j.matpr.2019.12.205
6. Xu, S., Gao, F., Han, J., Xiong, S., Duan, X., Zha, F., Yu, B. et al. (2022). Corrosion Behaviors of Fe-22Cr-16Mn-0.55N High-Nitrogen Austenitic Stainless Steel in 3.5% NaCl Solution. Coatings, 12 (11), 1769. https://doi.org/10.3390/coatings12111769
7. Jiang, G., Wu, M., Yang, X., Wang, H., Zhu, Y. (2024). Effect of Mn addition on microstructure and mechanical properties of $GX_{40}CrNiSi_{25\text{-}12}$ austenitic heat resistant steel. China Foundry, 21 (3), 205–212. https://doi.org/10.1007/s41230-024-3134-6
8. Nayak, C., Anand, A., Kamboj, N., Kantonen, T., Kajander, K., Tupala, V. et al. (2024). Tribological behavior and biocompatibility of novel Nickel-Free stainless steel manufactured via laser powder bed fusion for biomedical applications. Materials & Design, 242, 113013. https://doi.org/10.1016/j.matdes.2024.113013
9. Xu, N., Chen, G., Zhang, Q., Hu, H., Xu, G. (2025). Study on the Deformation Behavior and Mechanical Properties of Lightweight Economic Stainless Steels with Varying Al and Mn Contents. Journal of Manufacturing and Materials Processing, 9 (7), 206. https://doi.org/10.3390/jmmp9070206
10. Patra, S., Agrawal, A., Mandal, A., Podder, A. S. (2021). Characteristics and Manufacturability of Duplex Stainless Steel: A Review. Transactions of the Indian Institute of Metals, 74 (5), 1089–1098. https://doi.org/10.1007/s12666-021-02278-7
11. Li, Z., Luo, H., Hou, L., Zhao, Q., Wang, X., Chang, Y. (2025). Effect of Mn addition on the corrosion behavior of FeCrNiMn Si alloys in simulated seawater environment. Corrosion Science, 252, 112978. https://doi.org/10.1016/j.corsci.2025.112978
12. Hsu, K.-M., Chien, W.-L., Lin, C.-S. (2023). The improved stability and corrosion resistance of the passive film on Mn-containing FeCrNiCoMnx high entropy alloys by multiple pickling. Journal of Alloys and Compounds, 962, 171141. https://doi.org/10.1016/j.jallcom.2023.171141
13. Wang, Z., Yan, Y., Wu, Y., Zhang, Y., Zhao, X., Su, Y., Qiao, L. (2023). Recent research progress on the passivation and selective oxidation for the 3d-transition-metal and refractory multi-principal element alloys. Npj Materials Degradation, 7 (1). https://doi.org/10.1038/s41529-023-00410-0
14. Kartikasari, R., Kadiman, S., Muhfidin, R., Aziz, I., Triyono, T. (2024). Development of Fe-Cr-C alloys with high Mn content for bone implant. Eastern-European Journal of Enterprise Technologies, 5 (12 (131)), 31–38. https://doi.org/10.15587/1729-4061.2024.312442
15. Kartikasari, R., Subardi, A., Muhfidin, R., Aziz, I., Effendy, M., Triyono, T., Diharjo, K. (2023). Development of Fe-13.8Cr-8.9Mn alloy for steel biomaterials. Eastern-European Journal of Enterprise Technologies, 6 (12 (126)), 6–15. https://doi.org/10.15587/1729-4061.2023.293009
16. Ladani, L., Palmieri, M. (2024). Review of the Use of Metals in Biomedical Applications: Biocompatibility, Additive Manufacturing Technologies, and Standards and Regulations. Metals, 14 (9), 1039. https://doi.org/10.3390/met14091039
17. Romanczuk-Ruszuk, E., Krawczyńska, A., Łukaszewicz, A., Józwik, J., Tofil, A., Oksiuta, Z. (2023). Bioactivity, Cytotoxicity, and Tribological Studies of Nickel-Free Austenitic Stainless Steel Obtained via Powder Metallurgy Route. Materials, 16 (24), 7637. https://doi.org/10.3390/ma16247637
18. Bosch, J., Martin, U., Aperador, W., Bastidas, J. M., Ress, J., Bastidas, D. M. (2021). Corrosion Behavior of High-Mn Austenitic Fe–Mn–Al–Cr–C Steels in NaCl and NaOH Solutions. Materials, 14 (2), 425. https://doi.org/10.3390/ma14020425
19. Jung, J., Ma, B. (2002). Pat. No. US8043446B2. High manganese duplex stainless steel having superior hot workabilities and method manufacturing thereof. Available at: https://patents.google.com/patent/US8043446B2/en
20. Yu, K. P., Jiang, H., Xu, X. Y., Huang, M. X. (2024). Design of corrosion-resistant alloys for preventing oxidation-induced nanoscale Cr-depletion by inclusion engineering. Materials & Design, 244, 113146. https://doi.org/10.1016/j.matdes.2024.113146
21. Eliaz, N. (2019). Corrosion of Metallic Biomaterials: A Review. Materials, 12 (3), 407. https://doi.org/10.3390/ma12030407
22. Rybalchenko, O., Anisimova, N., Martynenko, N., Rybalchenko, G., Belyakov, A., Shchetinin, I. et al. (2023). Biocompatibility and Degradation of Fe-Mn-5Si Alloy after Equal-Channel Angular Pressing: In Vitro and In Vivo Study. Applied Sciences, 13 (17), 9628. https://doi.org/10.3390/app13179628

23. Ribeiro, J. J. K., Turin, A. R., Nuñez de la Rosa, Y. E., Quadros, P. V. C. A., Calabokis, O. P., Lepienski, C. M. et al. (2023). Mechanical Characterization at Nanoscale of Austenite, Ferrite, and Sigma Phases via Hardness Measurement and Fretting Wear Behavior of a Duplex Stainless Steel. Metals, 13 (5), 864. https://doi.org/10.3390/met13050864
24. Omiogbemi, I. M.-B., Yawas, D. S., Das, A., Afolayan, M. O., Dauda, E. T., Kumar, R. et al. (2022). Mechanical properties and corrosion behaviour of duplex stainless steel weldment using novel electrodes. Scientific Reports, 12 (1). https://doi.org/10.1038/s41598-022-26974-6
25. Liu, S., Ge, Y., Liu, H., Liu, J., Feng, Y., Chen, C., Zhang, F. (2022). Tensile Properties and Microstructure Evolutions of Low-Density Duplex Fe–12Mn–7Al–0.2C–0.6Si Steel. Materials, 15 (7), 2498. https://doi.org/10.3390/ma15072498
26. Yan, X., Wu, Y., Zhang, M., Liu, S., Sun, L., Feng, Y. (2022). Microstructure Evolution and Mechanical Properties of Ferrite–Austenite Duplex Fe-Mn-Al-(Cu)-C Steel under Different Annealing Temperatures. Materials, 15 (22), 8271. https://doi.org/10.3390/ma15228271
27. Zhang, C., Bao, X., Hao, M., Chen, W., Zhang, D., Wang, D. et al. (2022). Hierarchical nano-martensite-engineered a low-cost ultra-strong and ductile titanium alloy. Nature Communications, 13 (1). https://doi.org/10.1038/s41467-022-33710-1
28. Du, C., Wang, X. (2025). Intergranular precipitation evolution and its effect on the impact toughness of Super304H austenitic stainless steel weld metal during long-term aging at 650°C. Journal of Materials Research and Technology, 36, 7304–7317. https://doi.org/10.1016/j.jmrt.2025.04.312
29. Misra, R. D. K. (2023). A perspective in the understanding of strength–toughness combination during processing of engineering ferrous alloys. Materials Technology, 38 (1). https://doi.org/10.1080/10667857.2023.2278000
30. He, J., Lv, J., Song, Z., Wang, C., Feng, H., Wu, X. et al. (2023). Maintaining Excellent Mechanical Properties via Additive Manufacturing of Low-N 25Cr-Type Duplex Stainless Steel. Materials, 16 (22), 7125. https://doi.org/10.3390/ma16227125
31. Maier, A., Rühr, M., Stephan, M., Frankl, S., Roth, S., Schmidt, M. (2023). Tailoring material properties of duplex stainless steel by DED-LB/M and in situ alloying with elemental powders. Journal of Laser Applications, 35 (4). https://doi.org/10.2351/7.0001119
32. Ma, H., Zhao, Y., Feng, Y., Yu, Z., Sun, J., Song, H. et al. (2024). Effect of Mn content on corrosion and mechanical behaviors of Fe-based medium entropy alloy. Journal of Materials Research and Technology, 30, 5632–5651. https://doi.org/10.1016/j.jmrt.2024.04.246